# Tracing Morphological Transformations and Braiding Dynamics in the Himalayan Rivers of Nepal

Bhatta, Bishwas; Singh, Umesh; Adhikari, Basanta Raj; Karki, Saroj; Bhatta, Astha

**DOI**
10.1016/j.rsase.2025.101705

**Publication date**
2025

**Document Version**
Final published version

**Published in**
Remote Sensing Applications: Society and Environment

**Citation (APA)**
Bhatta, B., Singh, U., Adhikari, B. R., Karki, S., & Bhatta, A. (2025). Tracing Morphological Transformations and Braiding Dynamics in the Himalayan Rivers of Nepal. *Remote Sensing Applications: Society and Environment*, *39*, Article 101705. https://doi.org/10.1016/j.rsase.2025.101705

Remote Sensing Applications: Society and Environment 39 (2025) 101705

Contents lists available at ScienceDirect

Remote Sensing Applications: Society and Environment

journal homepage: www.elsevier.com/locate/rsase

# Tracing Morphological Transformations and Braiding Dynamics in the Himalayan Rivers of Nepal

Bishwas Bhatta [a,*], Umesh Singh [b], Basanta Raj Adhikari [a], Saroj Karki [c], Astha Bhatta [d]

[a] Department of Civil Engineering, Pulchowk Campus, Tribhuvan University, Nepal
[b] Hydrolab Private Limited, Lalitpur, Nepal
[c] Ministry of Water Supply, Irrigation and Energy, Biratnagar, Koshi Province, Nepal
[d] Delft University of Technology, Delft, Netherlands

ARTICLE INFO

*Keywords:*
Hydro-morphological monitoring
Braided rivers
Planform adjustment
Braiding intensity
Sandbar evolution
Remote sensing
Himalayan rivers

ABSTRACT

This study quantifies multi-decadal (1990–2022) planform change and braiding behavior in three Himalayan rivers of Nepal: The Koshi, Narayani, and Karnali using a unified geospatial workflow. Multi-temporal Landsat and Sentinel-2 imagery were processed with water-detection indices (MNDWI, NDWI) to extract channel boundaries and map erosion, accretion, and persistence. High-frequency gauge records were used to derive discharge and examine functional relations between wetted-area ratio and flow, and 180 Sentinel-2 scenes (2017–2022) supported braiding-intensity ($BI_{T3}$) estimation and bar-scale assessment at sub-reach level. Results show strong river-specific contrasts: the Koshi exhibits the greatest adjustment, with only 32.5 % channel persistence and a pronounced westward lateral migration, whereas the Narayani and Karnali are comparatively stable, with 64.8 % and 54.5 % unchanged areas, respectively. Functional analyses indicate distinct sensitivities of wetted-area ratio to daily maximum discharge, and braiding intensity peaks at intermediate flows before attenuating at higher discharges. Focused sandbar analysis (2017–2022) in the Koshi reach reveals persistent bifurcation asymmetry and directional bar migration, consistent with post-monsoon redistribution of flow and sediment. By linking satellite-derived morphology to real-time discharge within a consistent, transferable framework, the study provides robust, repeatable indicators for monitoring Himalayan braided rivers and establishes a basis for comparative evaluation of planform stability and braiding across data-sparse systems.

## 1. Introduction

Rivers evolve under varying hydrological, sedimentary, and boundary conditions, resulting in diverse morphological patterns across different fluvial systems (Eaton et al., 2010; Li et al., 2022). Among these, braided rivers exhibit particularly dynamic and intricate behavior, characterized by rapid adjustments in channel form, sediment distribution, and bar formation due to fluctuating discharge, high sediment supply, and erodible banks composed of non-cohesive materials (Ashmore, 2013; Bertoldi, 2021; Surian,

* Corresponding author.
*E-mail addresses:* 078mswre003.bishwas@pcampus.edu.np (B. Bhatta), umesh.hydrolab@gmail.com (U. Singh), bradhikari@ioe.edu.np (B.R. Adhikari), sarojioe@gmail.com (S. Karki), a.bhatta-1@tudelft.nl (A. Bhatta).

https://doi.org/10.1016/j.rsase.2025.101705
Received 8 December 2024; Received in revised form 24 August 2025; Accepted 26 August 2025
Available online 28 August 2025

2015). These rivers are known for frequent channel shifting, bank erosion, and floodplain reworking, processes that can have substantial socio-environmental implications (Belayneh et al., 2020; Dabojani et al., 2014; Yigez et al., 2021).

Despite considerable advances in understanding river morphology, accurately predicting planform evolution in braided rivers remains a challenge due to their non-linear, self-organizing behavior and strong sensitivity to both natural and anthropogenic drivers (Boota et al., 2021). External influences such as climate change, land use transitions, seismic disturbances, and changing hydrological regimes further complicate efforts to interpret and forecast their behavior (Baniya et al., 2023; Grill et al., 2019; van Vliet et al., 2013). Additionally, local controls such as sediment grain size, vegetation cover, and bank composition exert considerable influence on braided river stability and morphological response (Tockner et al., 2006). These complexities underscore the need for spatially and temporally explicit tools to capture morphological variability and change (Chalov and Alexeevsky, 2013). Remote sensing (RS) and geographic information systems (GIS) can be used to underpin quantitative analyses of river planform dynamics, providing cost-effective, basin-scale, multi-decadal observations from consistent satellite archives (Nones, 2021). When synoptic imagery is integrated with reproducible GIS workflows, it enables rigorous extraction of channel and water extents, derivation of bar metrics, and robust change detection across time (Tomsett and Leyland, 2019). This RS-GIS framework supports erosion-accretion mapping, coupling of morphology with discharge variability, and assessment of land-use impacts, thereby strengthening routine monitoring and decision support for river management (Ibitoye, 2021; Yaraghi et al., 2019). Within this context, Google Earth Engine (GEE) has become a pivotal cloud platform, unifying long-term Earth observation archives with scalable, on-demand computation (Gorelick et al., 2017). By enabling rapid preprocessing, index calculation, and temporal compositing over large areas, GEE reduces data and processing barriers while enhancing methodological consistency. In this study, its integration of high-resolution datasets is pivotal for analyzing fluvial morphology in data-sparse or logistically challenging regions, supporting multi-decadal, multi-basin, cross-reach comparisons of braided-river adjustments under variable hydrologic regimes.

Braided-river planform evolution reflects the combined influence of hydrological, sedimentary, tectonic, and human forcing. Channel adjustment processes including bed aggradation and degradation, lateral migration, channel widening or narrowing, and avulsion are driven by variations in sediment supply (both quantity and grain-size/composition) and by the timing and magnitude of flows associated with an intense monsoon regime; recurrent seismic activity and anthropogenic interventions further modulate these responses (Devreux et al., 2022; Saikia et al., 2024).Consequently, braided systems exhibit rapid, non-linear shifts in morphology in response to flood pulses. Channel position and morphology shift even during moderate discharge events, but these changes being complex and non-linear, requires discharge data alongside RS to fully understand river dynamics (Hooke, 2023). Understanding

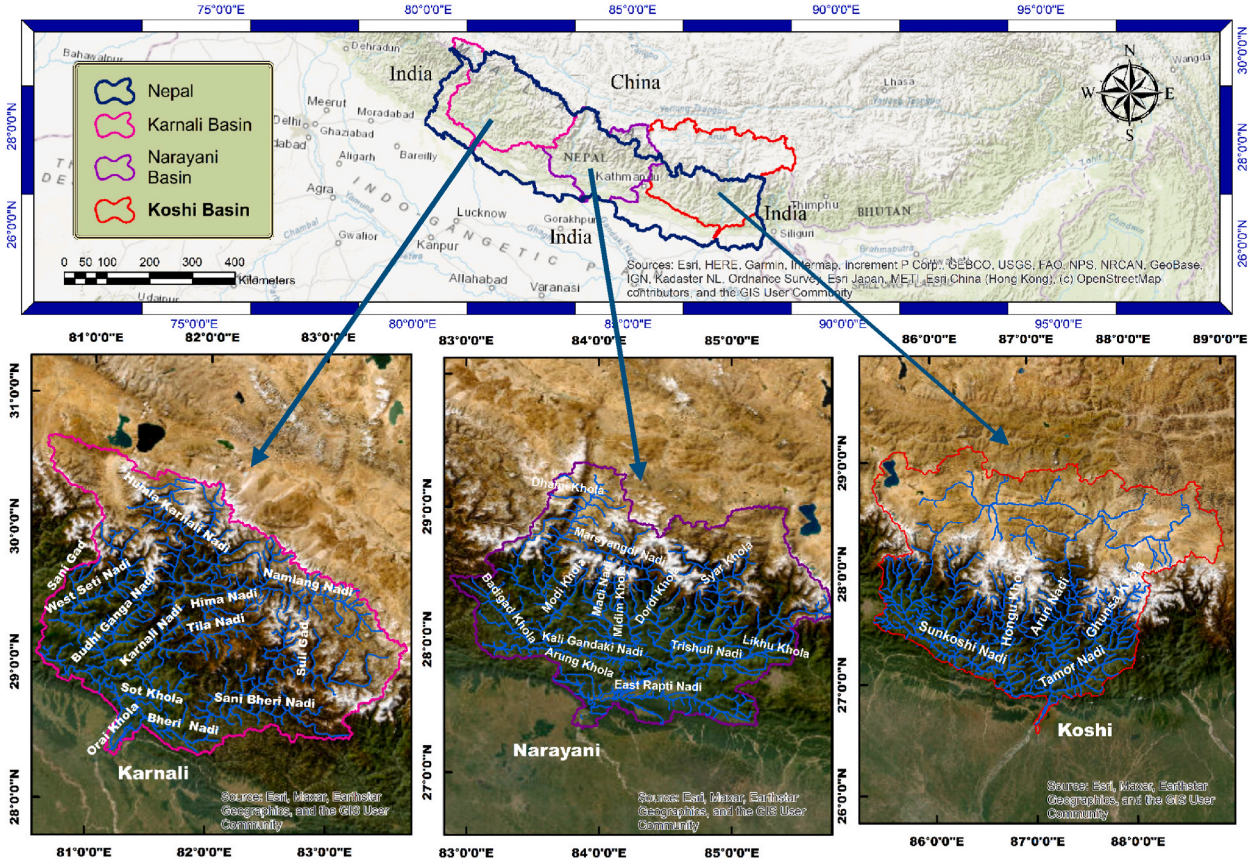


**Fig. 1.** Location map showing the catchment areas of the three Himalayan rivers.

braided river systems requires a comprehensive examination of key morphological processes such as erosion, deposition, channel migration, and irregular planform formation, all of which are significantly influenced by the variability in stream power (Pradhan et al., 2021). Despite extensive work on braided-river morphology, quantitative coupling of planform metrics with real-time discharge across multiple Himalayan systems remains limited. Previous studies have largely focused on single reaches or short-term events, often relying on heterogeneous datasets. As a result, non-monotonic responses such as peak braiding at intermediate flows, or reach-specific thresholds linked to bar drowning, channel consolidation, and lateral migration, remain less well explored. A systematic, cross-basin comparison using consistent imagery, harmonized metrics, and concurrent hydrological records would therefore provide valuable insights into the drivers of instability and highlight regions most vulnerable to morphological change.

Addressing this gap, the present study delivers a comparative, multi-decadal (1990–2022) assessment of the Koshi, Narayani, and Karnali rivers by integrating Landsat and Sentinel time series with rating-curve-derived discharge. A unified geospatial workflow is introduced to (i) extract erosion, accretion, and unchanged zones; (ii) quantify braiding intensity ($BIT_3$), planform persistence, and sinuosity; and (iii) evaluate functional relationships between wetted-area ratio ($R_W$), discharge, and braiding, including threshold behavior. A focused six-year analysis of sandbar evolution in the Koshi reach further resolves bifurcation asymmetry and directional bar migration under post-monsoon conditions. Collectively, the framework provides a transferable, data-efficient basis for diagnosing morphological adjustment in data-sparse braided rivers and for prioritizing reaches most susceptible to change.

## 2. Study area

The Nepal Himalaya is characterized by several major river basins, which are vital for the region's hydrology, ecology, and human livelihoods (Karki et al., 2023). Among the prominent river systems, the Koshi, Narayani, and Karnali basins (Fig. 1) stand out as the most significant due to their size, geographic distribution, and socio-economic importance.

**Koshi River System:** Originating in the eastern Himalayas, this river system covers a vast drainage area across Nepal and China. A 42 km reach from Chatara to the Koshi barrage having a gradient of 1:2000 (Neupane et al., 2022) is the focus of this study due to its significant braiding patterns, sediment transport processes, and flood dynamics, influenced by the diverse terrains of the Himalayan, Mahabharat, and Siwalik ranges. This area carries nearly 100 Mt/yr of sand-gravel bedload, sourced from active headwater erosion (Hovius et al., 1997). The average annual sediment load at Chatara was estimated at 130 million $m^3$, with nearly 60 million $m^3$ as bed material load (Kafle, 2019). Quartz and feldspar dominate Koshi River sediments, with feldspar/quartz ratios declining from 0.55 upstream to 0.37 downstream while higher upstream calcite (12 %) versus downstream dolomite (3 %) suggesting weaker chemical weathering in the upper reaches (Mingyue et al., 2019). Riparian strips are sparse seasonal grasses and shrubs offering minimal bank cohesion (Kafle, 2021). The Koshi River basin has a mean basin relief of 2.2 km and receives an average annual rainfall of 920 mm (Andermann et al., 2012). Across the entire Koshi Basin, the contribution from snow and glacier melt at the Chatara station, a key downstream hydrological outlet is estimated to be approximately 12 % of the annual streamflow (Chhetri et al., 2021). The Koshi Basin experiences four seasons: pre-monsoon, monsoon, post-monsoon, and winter with significant spatial and temporal variations in water balance; average annual precipitation is highest in the Central (about 1775 mm) and Eastern mountain regions (around 1418 mm) and lowest in the Trans-mountain region (about 210 mm), resulting in approximately 71 % of annual flow during the monsoon, while evapotranspiration exceeds runoff in upper sub-basins and runoff dominates in the lower sub-basins (Bharati et al., 2016). The presence of a real-time discharge station number 695 established by the Department of Hydrology and Meteorology (DHM) at Chatara enhances the ability to monitor hydrological variations and their impacts on river morphology.

**Narayani River System:** This central Nepal river system is a major tributary to the Ganges, with a drainage area of 46,300 $km^2$, of which 31,100 $km^2$ lies within Nepal (Bajracharya et al., 2015). The selected 54 km reach from Devghat to Baguban lies downstream of major tributary confluences creating highly variable flow and sediment-transport regimes. Channel beds range from coarse sand to fine gravel with the percentage of gravel notably higher in upstream and midstream segments, while sand dominated in downstream reaches (Jha et al., 2010) and the riparian zone along the Narayani River supporting diverse vegetation, including over 230 plant species dominated by grasses (Saccharum spontaneum, Imperata cylindrica), legumes, and Asteraceae species, which contribute to partial bank stabilization and influence floodplain dynamic. The basin has a mean basin relief of 2.3 km and receives an average annual rainfall of 1396 mm (Andermann et al., 2012). Gauge no.450 monitors real-time flows. The system's connectivity with the Ganges Basin underscores its significance in transboundary water management and flood mitigation strategies.

**Karnali River System:** As the longest river in Nepal, the Karnali River traverses the western region with a fan-shaped topography crucial for studying sediment deposition and floodplain dynamics, being one of the largest depositional landforms in Nepal (MacClune et al., 2014). Originating in western Tibet, it drains 45,440 $km^2$ and spreads into a megafan south of the Churia Range. The 45 km reach from the Karnali Bridge to Kailashpuri Dam descends from 260 m to 139 m above mean sea level (Rakhal et al., 2021). Beds are dominated by coarse gravel and cobbles, vegetated mid-channel bars support shrubs and young trees that afford only limited bank resistance (Kafle, 2021). The basin has a mean basin relief of 2.1 km and receives an average annual rainfall of 920 mm (Andermann et al., 2012).

Together, these river systems not only shape the physical landscape of Nepal but also play a vital role in the hydrological regime of the larger Ganges River Basin. Their study is crucial for addressing regional water security challenges, understanding sediment transport dynamics, and implementing sustainable river management practices. The diverse hydrological characteristics and geographical contexts of the Koshi, Narayani, and Karnali rivers make this study area particularly captivating for research on riverine processes and their implications for both local and regional environmental management.

## 3. Materials and methodology

### 3.1. Materials

A detailed analysis of river morphological dynamics was conducted using a workflow that combined image processing and spatial analysis techniques (Fig. 2). For this, Landsat 5 Thematic Mapper (TM), Landsat 8 Collection 1 Tier 1 Surface Reflectance, Landsat 9 Collection 2 Tier 1 Top-of-Atmosphere (TOA), and Sentinel-2A satellite images were selected. The Landsat series, offering a 30-m spatial resolution, were selected for their consistent temporal coverage from 1990 to 2022. Sentinel-2A imagery, with a 10-m spatial resolution was most prioritized and was utilized for recent, high-precision analysis, particularly useful for capturing finer morphological details such as river braiding (Yang et al., 2020). However, Landsat imagery was also used in cases where Sentinel-2 scenes were affected by excessive cloud cover. All imagery was accessed and processed on the Google Earth Engine (GEE) platform using the JavaScript API, which supports efficient handling of large geospatial datasets (Azzari and Lobell, 2017; Gorelick et al., 2017). Image selection prioritized cloud-free conditions within the post-monsoon period. For real-time discharge data, high-frequency gauge measurements were obtained from the DHM of Nepal, recorded at 10-min intervals for the Koshi River, 5-min intervals for the Narayani River, and 15-min intervals for the Karnali River.

### 3.2. Methodology

Imagery acquisition was timed to the post-monsoon, post-flood season, a period characterized by hydrological stability and reduced cloud cover, which optimizes the delineation of channel morphology. Spectral indices were employed for waterbody extraction, beginning with the Normalized Difference Water Index (NDWI) introduced by Mcfeeters (1996), which utilizes the green and near-infrared bands to extract water bodies. Building on this, the Modified Normalized Difference Water Index (MNDWI), proposed by Xu (2006), incorporates the green and shortwave infrared (SWIR) bands, offering improved accuracy in distinguishing water bodies from features such as shadows (Singh et al., 2015). Hence, MNDWI was chosen for Landsat imagery, MNDWI was calculated using the

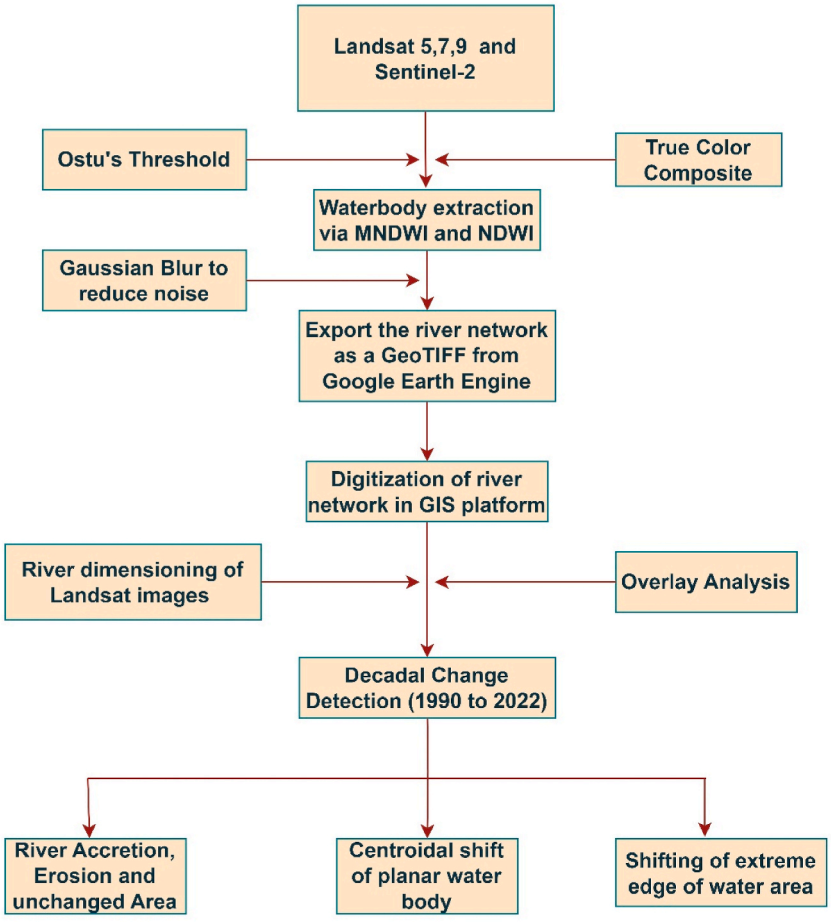


**Fig. 2.** Methodological framework for assessing river channel migration.

formula

$$MNDWI = \frac{\text{Green} - \text{SWIR}}{Green + \text{SWIR}} \quad (1)$$

However, the use of MNDWI for Sentinel-2A images due to its SWIR band being 20 m resolution results spatial resolution of 20 m. But the use of NDWI yields 10 m resolution as both green and NIR bands have resolution of 10 m. So, for obtaining higher spatial resolution from Sentinel-2A image, NDWI has been used using formula

$$\text{NDWI} = \frac{\text{Green} - \text{NIR}}{\text{Green} + \text{NIR}} \quad (2)$$

An optimal threshold value to distinguish water bodies from other land cover types can be calculated using Otsu threshold method (Xu et al., 2011). So, the use of both the Otsu's method and visual inspection of the composed true color image has been done to set NDWI and MNDWI values ensuring that only water bodies are included in the analysis. To enhance image quality, a Gaussian kernel was employed to apply a smoothing filter. This approach effectively mitigated noise and minimized small-scale variations, thereby improving the visual clarity and definition of water features in the image (Dyson et al., 2024).

Thus, obtained waterbodies were extracted as river networks and exported as GeoTIFF files, a versatile raster data format that retains spatial resolution and georeferencing information. These files were then imported into a GIS platform, where the river networks were digitized for detailed analysis. Overlay analysis was conducted to identify erosion, accretion, and unchanged areas. Erosion areas were defined as regions where land was lost due to water body expansion. Accretion areas were characterized by sediment deposition in previously water-covered zones, which no longer experienced flow in the studied time periods. Unchanged areas were regions where the flow path remained consistent between the decadal intervals. By intersecting the relevant feature classes, a new feature class was created to capture the overlapping areas. This process facilitated the extraction of unchanged areas.

To analyze river morphology at a finer scale, it was essential to characterize the braiding patterns and correlate it with upstream discharge in the studied reach. To achieve this, rating curves were developed using real-time gauge height data from the Koshi, Narayani, and Karnali rivers (Fig. 3). The rating curve formulated using equation $Q = k(H-H_0)^n$ was employed, where Q is the discharge, H is the gauge height, $H_0$ is the reference gauge height, and k and n are curve-fitting parameters.

To optimize these parameters, the Generalized Reduced Gradient (GRG) nonlinear solver was employed due to its robustness (Smith and Lasdon, 1992), iteratively adjusting them to minimize the discrepancy between observed and predicted discharge values, in accordance with the least squares fitting method (Mir and Dubeau, 2015). The accuracy of the rating curve was rigorously evaluated using statistical metrics such as the Nash-Sutcliffe Efficiency (NSE), Root Mean Square Error (RMSE), and the correlation coefficient (r). These metrics provided a comprehensive assessment of the rating curve's predictive performance, ensuring its reliability for estimating discharge based on gauge height data.

The performance of the method for parameter estimation was evaluated by analyzing the relation between the observed and the predicted discharge using the following statistics.

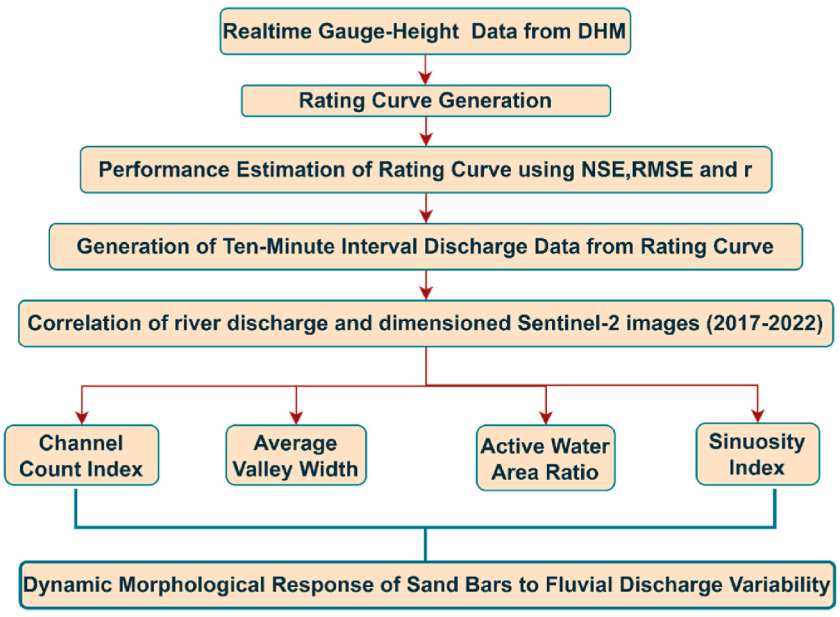


**Fig. 3.** Workflow diagram illustrating the use of rating curve and analyzing the dynamic morphological response of sand bars to fluvial discharge variability.

$$\mathrm{NSE} = 1 - \frac{\sum_{i}^{N}\left(Q_o^i - Q_p^i\right)^2}{\sum_{i}^{N}\left(Q_o^i - \overline{Q}\right)^2};\ \text{Nash} - \text{Sutliffe criteria(E)} \quad (3)$$

$$RMSE = \sqrt{\frac{\sum_{i}^{N}\left(Q_o^i - Q_p^i\right)^2}{N}};\ \text{Root Mean Square Error (RMSE)} \quad (4)$$

$$r = \frac{N\left(\sum Q_o Q_p\right) - \left(\sum Q_p\right)\left(\sum Q_o\right)}{\sqrt{\left(N\left(\sum Q_p^2\right) - \left(\sum Q_p\right)^2\right) - \left(N\left(\sum Q_o^2\right) - \left(\sum Q_o\right)^2\right)}};\ \text{Correlation coefficient} \quad (5)$$

where $Q_o$ is the observed discharge, $Q_p$ is predicted discharge and $\overline{Q}$ is mean observed discharge.

Further, total of 180 Sentinel-2 images, covering the years 2017–2022, were digitized and analyzed to quantify the braiding intensity of the rivers. This process enabled a thorough comparison of the morphological characteristics among the rivers and allowed for the identification of correlations between these characteristics and upstream continuous discharge data.

## 4. Results

### 4.1. Decadal study: morphological dynamics and channel shifts

The comparison across three distinct periods: 1990 to 2000, 2000 to 2010, and 2010 to 2022 reveals dynamic changes in erosion, accretion, and the planar extent of water bodies in the Koshi, Narayani, and Karnali River systems. Landsat-5 imagery was used for the first two periods, while Landsat-9 was used for the 2022 analysis. Waterbody delineation was performed using MNDWI and NDWI, with histogram-based Otsu's thresholding method applied on a clipped area specific to each river in order to identify optimal water non-water separation. The Otsu-derived thresholds were 0.0539 for Koshi, 0.0385 for Narayani, and 0.0700 for Karnali, and were further refined through visual inspection to ensure consistent mapping across time periods. The resulting classified images highlight distinct patterns of erosion and accretion along each river, shaped by both natural fluvial processes and human interventions over the past three decades.

#### 4.1.1. Koshi River in eastern Nepal

From 1990 to 2000, erosion measured 16.349 $km^2$, with 17.734 $km^2$ of accretion and 8.545 $km^2$ remaining unchanged. Subsequently, from 2000 to 2010, erosion increased to 18.138 $km^2$, with accretion rising to 21.773 $km^2$, and the unchanged area diminishing to 6.756 $km^2$. The latest comparison from 2010 to 2022 (Fig. 4) unveiled erosion covering 17.657 $km^2$, accretion expanding to 29.633 $km^2$, and an unchanged area of 10.872 $km^2$. These observations underscore the dynamic nature of the Koshi region's landscape, marked by significant shifts in erosion and accretion over time. The analysis indicates a significant westward migration in the mid-section of the Koshi river, likely driven by the construction of barrages and levees that have constrained the floodplain. Between 2000 and 2010, the cumulative westward shift reached up to 3871 m. This westward migration is further examined in the bar analysis section, discussed later in the paper.

#### 4.1.2. Narayani River at central Nepal

From 1990 to 2022, the Narayani river's centroid latitude remained stable, while longitude showed subtle shifts, with a notable 682 m shift in the planar water body between 2010 and 2022. From 1990 to 2000, erosion covered 12.892 $km^2$, accretion 9.278 $km^2$, and 10.774 $km^2$ remained unchanged. Between 2000 and 2010, erosion was 9.373 $km^2$, accretion 13.411 $km^2$, and 10.256 $km^2$ unchanged. In 2010–2022 (Fig. 5), erosion increased to 28.942 $km^2$, with 6.894 $km^2$ accretion and 12.735 $km^2$ unchanged. Also, it has gone significant shifts in its extreme bank channels. Notable changes include an 860 m northward shift and a substantial cumulative 1253 m southward shift from 1990 to 2000.

Similarly, from 2000 to 2010, remarkable shifts persisted, with a 901 m northward movement and a 1446 m northward shift. These trends continued from 2010 to 2022, with further noteworthy changes, 1001 m northward shift and a 657 m southward movement.

This dynamic interplay between minimal centroidal shift and notable edge movements indicates that while the overall flow area remains confined, the flow paths within this area exhibit a considerable degree of dynamism. In essence, the river's morphology appears to maintain a degree of stability in its central flow while simultaneously displaying dynamic and evolving behavior in its peripheral channels.

#### 4.1.3. Karnali River at western Nepal

From 1990 to 2000, the river exhibited significant erosional activity, with an erosion area of 21.559 $km^2$ and an accretion area of 15.123 $km^2$, while the unchanged area remained relatively stable at 15.517 $km^2$. In the following decade (2000–2010), erosion

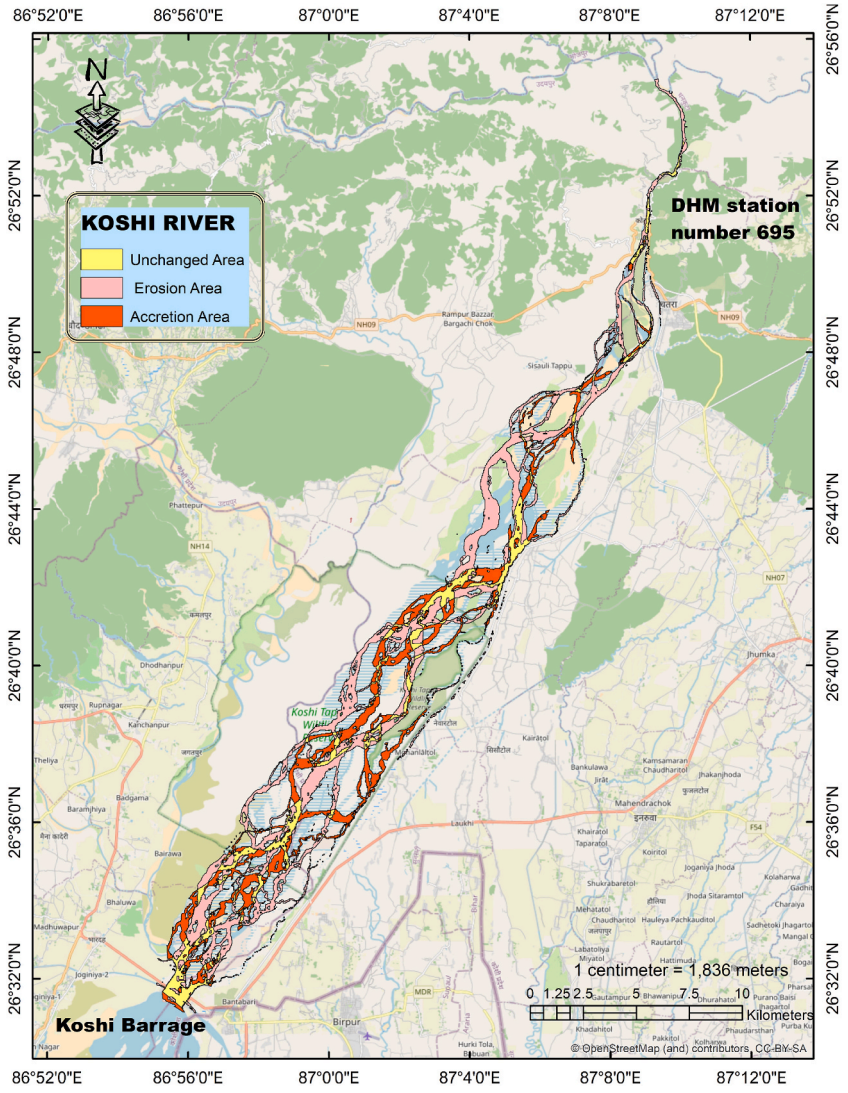


**Fig. 4.** Koshi River Channel Shift from 2010 to 2022, extending from upstream real-time discharge station no. 695 to the Koshi Barrage.

intensified, expanding to 30.37 km$^2$, with accretion at 15.62 km$^2$ and a slightly reduced unchanged area of 21.456 km$^2$. However, from 2010 to 2022(Fig. 6), this trend reversed, with erosion decreasing to 22.405 km$^2$, accretion increasing to 28.249 km$^2$, and the unchanged area measured at 23.577 km$^2$ (Fig. 7).

The channel shift analysis of the Karnali mega fan indicates a higher shift of the right branch compared to the left branch. The right branch predominantly displays a dominant westward shift, particularly noticeable in the upstream and middle sections, reaching as high as 2125 m. However, a notable eastward shift of 1732 m near the confluence of the two branches between 2010 and 2022 highlights a distinctive pattern attributed to the river's meandering behavior in that specific reach. Conversely, the left branch demonstrates a consistent westward shift, peaking at 1048 m. Notably, from 1990 to 2000, both branches exhibited significant shifts in their extreme bank channels. The subsequent decades further witnessed substantial shifts, with the left branch consistently shifting westward and the right branch encountering notable fluctuations, including substantial eastward shifts near the confluence. The increased shifting observed from 2010 to 2022 may be attributed to significant flooding events, such as those in 2010–2013 and 2014, leading to substantial alterations in the river's planform.

Additional analysis for the Karnali River mega fan was not conducted due to challenges in accurately quantifying discharge levels for its left and right branches. Discharge data is currently available only for the entire mega fan from real-time station number 280 at Chisapani.

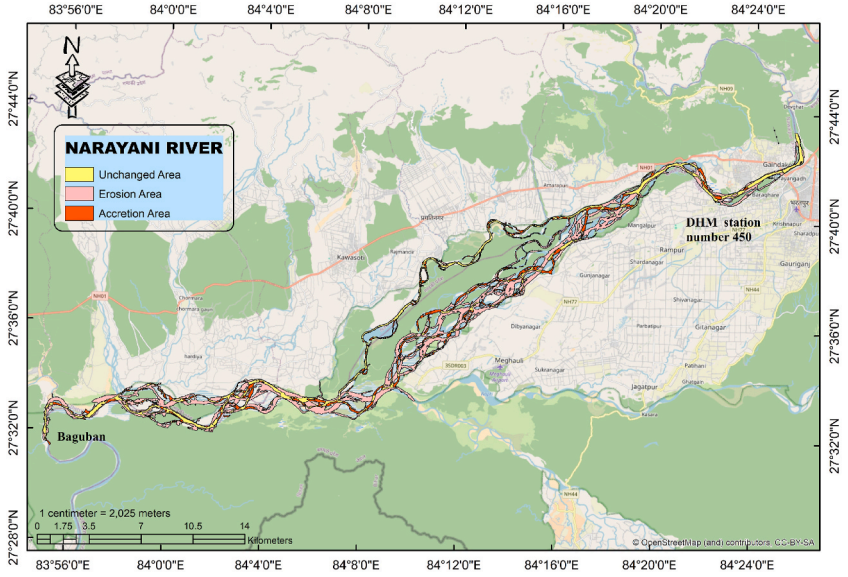


**Fig. 5.** Narayani River Channel Shift from 2010 to 2022, extending from upstream real-time discharge station no. 450 to the Baguban.

### 4.2. *Koshi and Narayani River braiding pattern analysis*

Utilizing the rating curve generation method recommended by Muzzammil et al. (2018), a total of 118 pairs of gauge height and discharge data were analyzed to develop a rating curve and estimate real-time discharge. The comparison between observed and predicted discharge, plotted using the rating curve equation, exhibited a strong correlation, particularly at higher discharge levels, underscoring the method's effectiveness. The obtained rating curve for Koshi river as $Q = 270.512(H\text{-}0)^{1.9679}$ was evaluated and performance yielded high statistical metrics, with an NSE of 0.9995, RMSE of 225.2, and an r-value of 0.9999, demonstrating a robust agreement between observed and predicted discharge values. This rating curve was subsequently applied to estimate discharge across various time periods, supporting further analysis. Moreover, the processing and digitization of 72 Sentinel-2 images from 2017 to 2022 enabled the extraction of critical parameters, including the date of image capture, wetted area, valley area, valley length, reach start-to-end straight length, and the total number of braids. For Narayani river, the rating curve generated from 104 pairs of gauge height and discharge data is $Q = 232.489\ (H\text{-}0)^{1.810}$. The rating curve equation used yielded a NSE of 0.9999, RMSE of 42.6, and a correlation coefficient (r) of 0.9999, demonstrating excellent agreement between observed and predicted discharge. The analysis includes processing and digitizing 55 Sentinel-2 images, chosen for minimal cloud coverage, from 2019 to 2022.

The Koshi River in the study area exhibits significant variation in wetted area, closely correlated with maximum discharge data over a six-year period. Notably, peak values occurred consistently in September, reaching up to 93.731 $km^2$, while the lowest wetted area was observed in March–April, with values as low as 27.665 $km^2$.This reflects a fluctuation of approximately 195.3 % when calculated relative to the maximum value, and 238.8 % when referenced from the minimum value. The relationship between the active water area ratio($R_W$) given by Li et al. (2020) and maximum discharge ($Q_{max}$) was modeled using a power function (Fig. 8), establishing a relation as $R_W = 0.0301Q_{max}^{0.2099}$ with an $R^2$ value of 0.8596. Similarly, Narayani river also showed strong logarithmic function as $R_W = 0.018\ln(Q_{max})\text{-}0.0743$ with $R^2$ value of 0.888.This strong correlation of established equation allows quantification of active water area since as river discharge increases, the active water area expands, though at a diminishing rate. This finding suggest that at higher discharges, the river's capacity to expand its wetted area is limited, which has significant implications for understanding channel morphology, floodplain interaction, and sediment transport dynamics within this river system.

The analysis of the average number of braids ($BI_{T3}$) (Hong and Davies, 1979) relative to the wetted area reveals a distinct trend: an initial increase in braiding intensity followed by a decline beyond a specific wetted area threshold (Fig. 9). Remarkably, both Koshi and Narayani River exhibit this distinct trend in their $BI_{T3}$. Unpredictably, even during periods of higher discharges in September, braiding intensity doesn't peak, which contrasts with previous findings (Egozi and Ashmore, 2008; Schuurman et al., 2018) that suggested increased branching during peak flow conditions. Furthermore, these findings are consistent with observations in the Yangtze River on the Qinghai-Tibet Plateau, as demonstrated in a study by Li et al. (2020), where a second-degree polynomial equation was established.

The fluctuating trend in $BI_{T3}$ values within the Koshi and Narayani rivers can be explained by analyzing the main channel's Sinuosity Index ($P_T$) (Mosley, 1981). The $P_T$ exhibits a decline with increasing discharge (Fig. 10), particularly after surpassing threshold discharge levels of approximately 2000 $m^3/s$ for the Koshi River and 1500 $m^3/s$ for the Narayani River. Notably, when discharge remains below these thresholds, $P_T$ experiences significant fluctuations for similar discharge values, followed by a consistent decline beyond these levels.

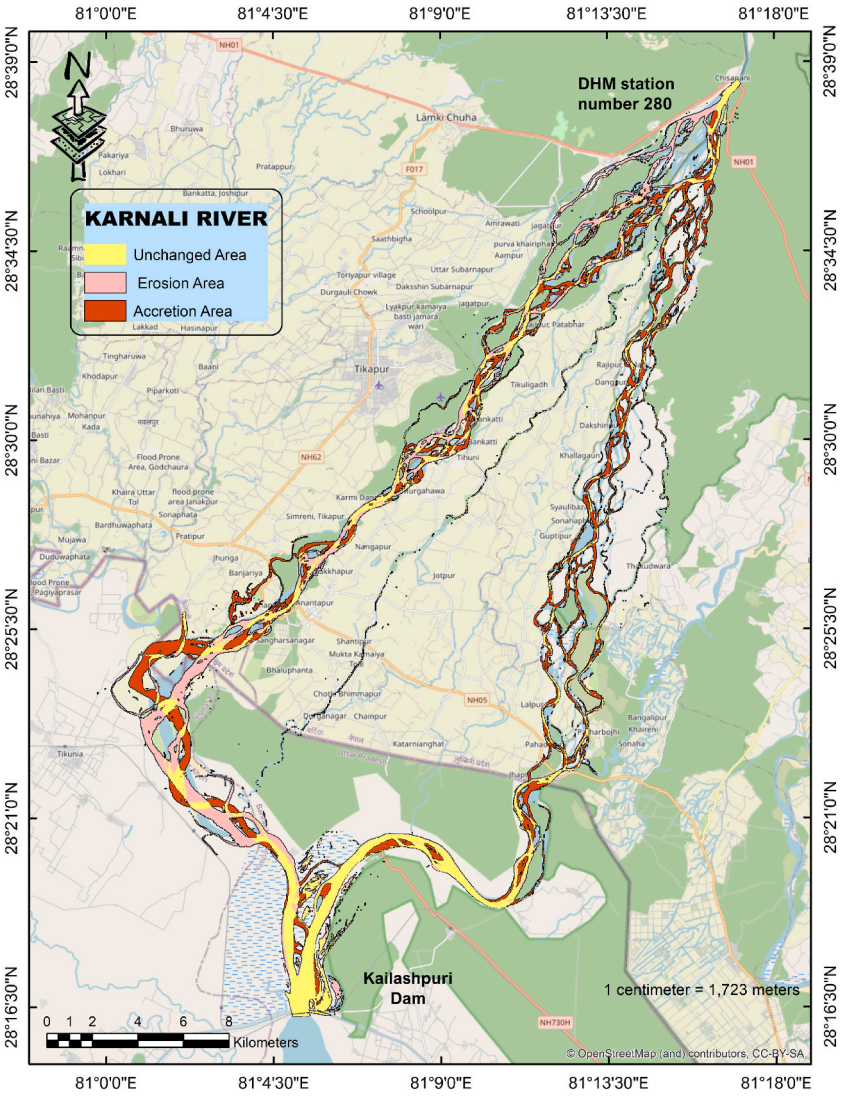


**Fig. 6.** Karnali River Channel Shift from 2010 to 2022, extending from upstream real-time discharge station no. 280 to the Kailashpuri Dam.

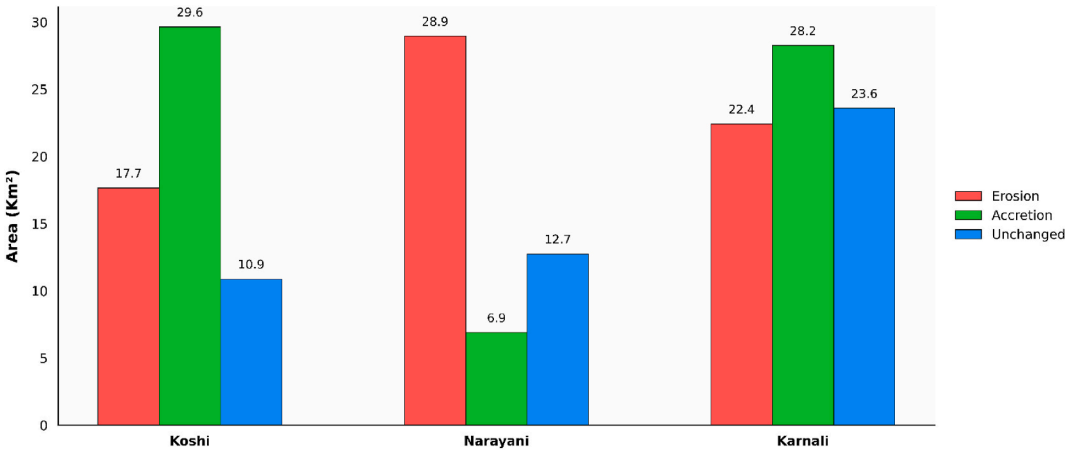


**Fig. 7.** Morphological changes in the Koshi, Narayani, and Karnali rivers from 2010 to 2022, showing quantified areas of erosion, accretion, and unchanged zones (in $km^2$).

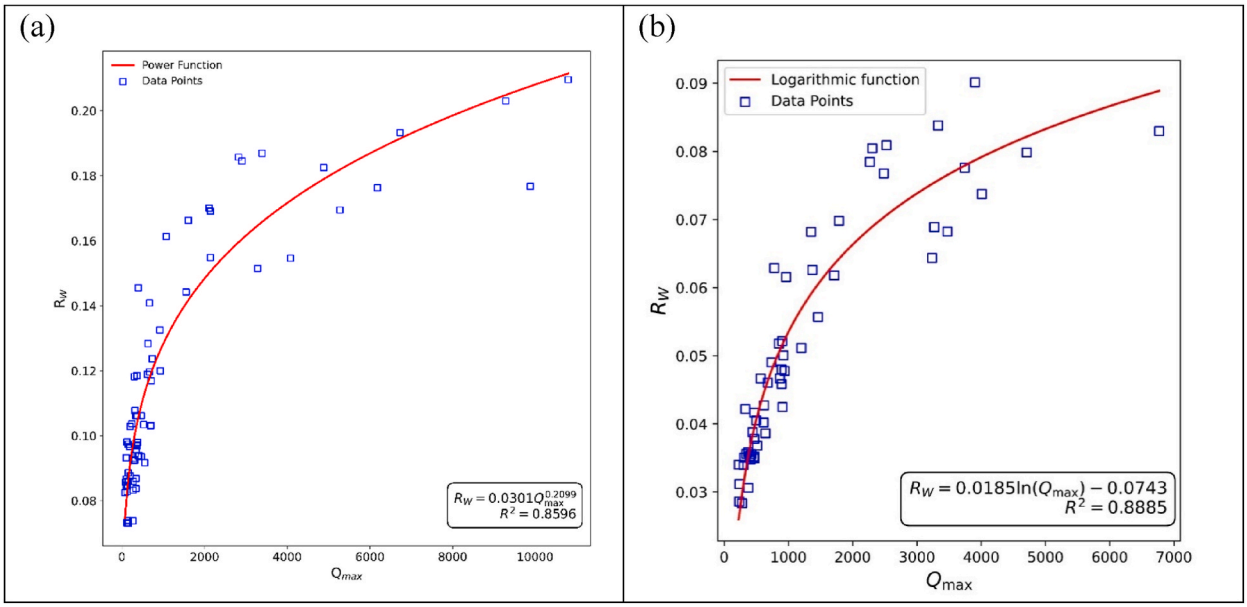


**Fig. 8.** Varying water area ratio ($R_W$) with daily maximum discharge ($Q_{max}$) in (a) Koshi and (b) Narayani River reach.

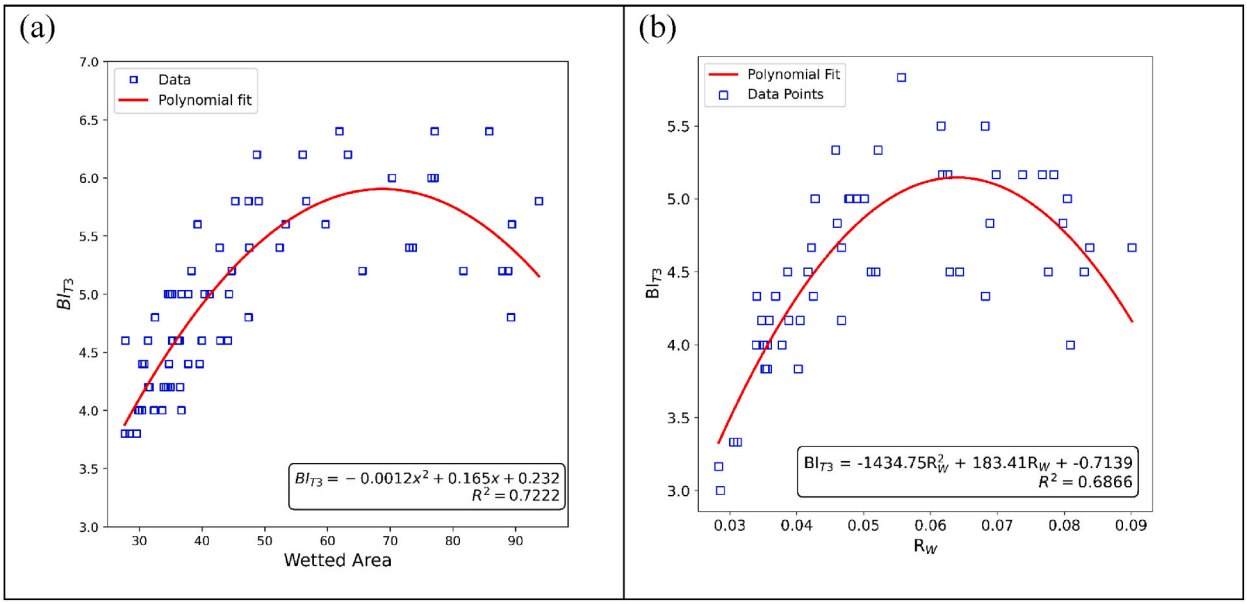


**Fig. 9.** (a) Relationship between braiding intensity ($BI_{T3}$) and wetted area in Koshi and (b) Relationship between $BI_{T3}$ and water area ratio ($R_W$) in Narayani River reach.

In these multi-threaded river systems, the impact of increased discharge on braiding can be understood through two primary mechanisms.

a) Braiding intensifies as new flow paths emerge, branching off from the main channel.
b) A reduction in braiding occurs due to the submersion, erosion, and removal of small sandbars from the main channel once the threshold discharge level is exceeded.

These interacting processes drive the observed braiding patterns. Braiding intensifies as new flow paths emerge, reaching a peak at wetted areas of around 70 $km^2$ for the Koshi river and 45 $km^2$ for the Narayani River. Beyond these areas, the continued erosion and displacement of sandbars dominate, leading to a reduction in braiding intensity as the wetted area expands.

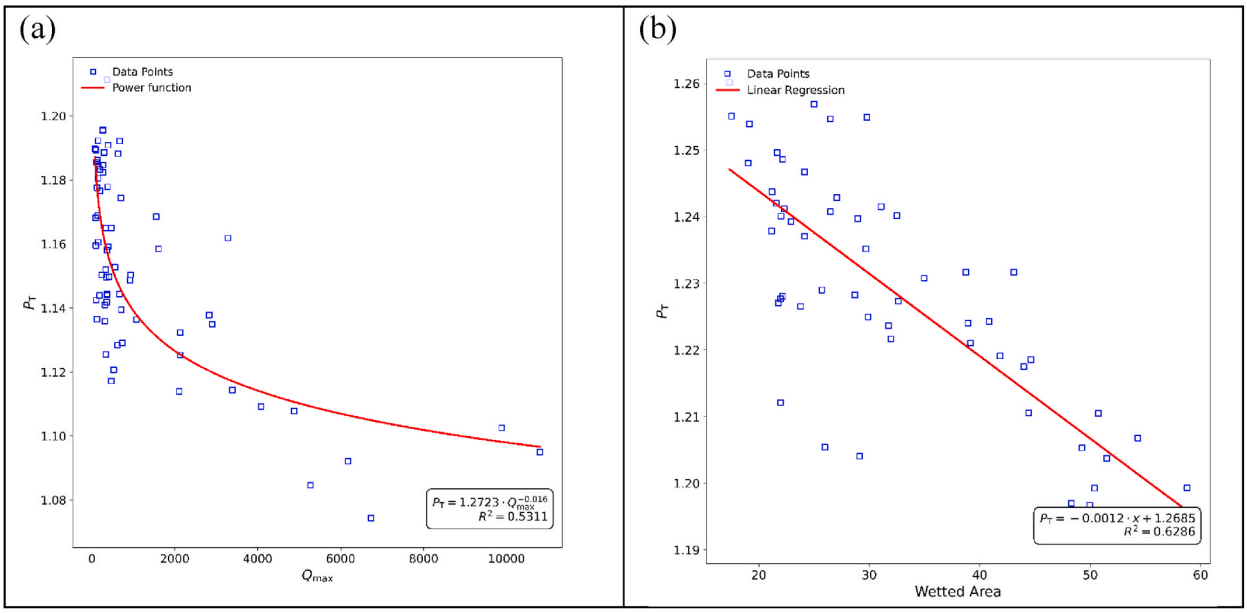


**Fig. 10.** Correlation between Sinuosity index ($P_T$) and daily maximum discharge (Qmax) in (a) Koshi and (b) $P_T$ and wetted area of Narayani River reach.

### *4.3. Quantifying sandbar responses to flood discharge variations in the Koshi River: temporal and spatial analysis (2017–2022)*

The Koshi River demonstrated a pronounced and recurrent westward migration trend, making it a focal point of geomorphological interest, which encouraged its selection for more detailed analysis. To further explore the persistent westward migration of the Koshi River, an in-depth analysis was performed over a six-year period from 2017 to 2022 where Sentinel-2 imagery from each November was selected to capture post-flooding conditions. Four key sandbars, located about 25 km upstream of the Koshi barrage, were identified as focal points for morphological change (Fig. 11). Changes in sandbar size, bifurcation angles, and river channel width were examined, and width asymmetry metric (Bertoldi, 2012) was used to quantify bifurcation as

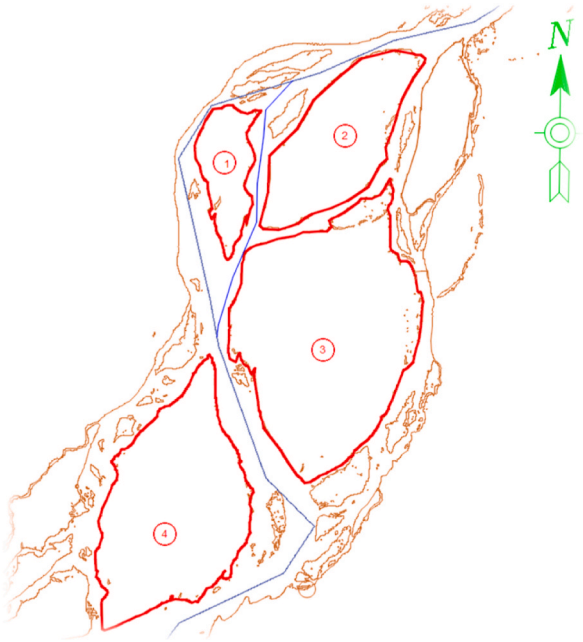


**Fig. 11.** Four major bars (outlined in red) selected for their contribution in changing channel morphology located about 25 km upstream of the Koshi Barrage.

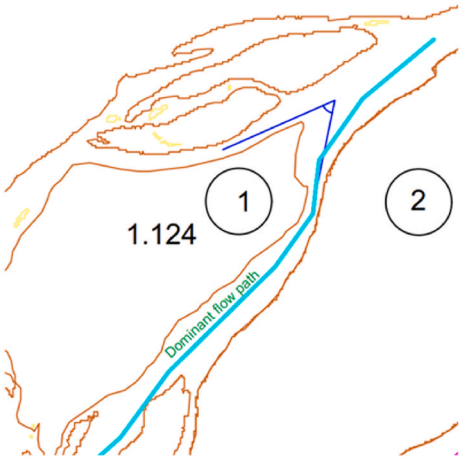


**Fig. 12.** Bar-1 with left dominant flow path.

$$\Delta B = \frac{W_L - W_R}{W_L + W_R} \quad (6)$$

A value of zero in this metric indicates a perfectly balanced bifurcation, while a value of one reflects a completely closed distributary. Positive values signify a left-dominant flow, whereas negative values indicate right-dominant flow. This approach helped quantify the river's shifting dynamics and the ongoing westward migration.

In 2017, bar-1 initially displayed a right-dominant flow, indicated by a ΔB value of −0.26. However, as the flooding discharge increased to 290 $m^3/s$ in 2018 and 3491 $m^3/s$ in 2019, a transition toward left-dominant flow emerged (Fig. 12), with ΔB values shifting to 0.06 and 0.12, respectively. This left-dominance remained consistent throughout the study period, as all subsequent ΔB values up to 2022 were positive.

Additionally, during this period, bar-1 demonstrated a consistent northeastward migration of its top central bar point, attributed to excessive sediment deposition following flooding events. This migration resulted in a cumulative shift of 1252 m, averaging 190.6 m per year (Fig. 13).

The upward movement and leftward shift of bar-1 are likely the primary drivers of the westward migration of the main river channel. This shift facilitates the bypassing of bar-1 by the flow, reinforcing the dominant flow pattern observed near bar-3. These changes highlight the complex interaction between sediment dynamics and channel morphology, emphasizing how alterations in one section of the river system can substantially influence downstream flow patterns and bar configurations.

The westward movement becomes more pronounced near bar-3. The plot of changes in ΔB3 with ΔQ exhibits a quadratic fit (Fig. 14). The flow path around bar-3 remained consistently right-dominant from 2017 to 2022 where from 2020 to 2021, notable increase in flooding discharge by 2865 $m^3/s$ resulted in a ΔB value of −0.56. This surge in discharge intensified the right-dominant flow, leading to bar splitting and the formation of a new right-dominant flow path (Fig. 15a).

This newly established path continues to evolve, reaching a ΔB of −0.52, which maintains the westward shift of the main channel. Moreover, it triggers the splitting of the recently formed sandbar (Fig. 15b). This splitting phenomenon is further amplified by the left-

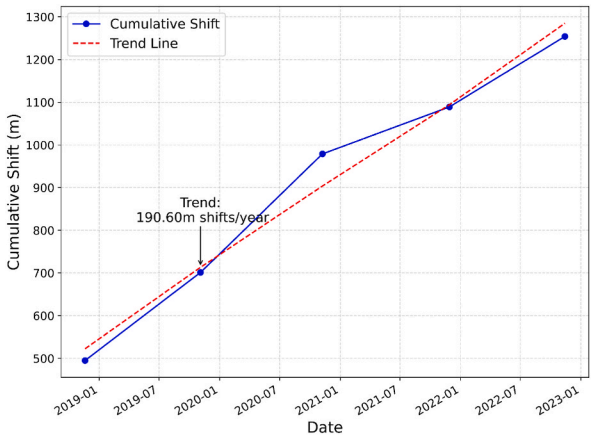


**Fig. 13.** Bar-1 of Koshi reach showcasing cumulative upward movement from 2017 to 2022 with an average shift of 190.6 m per year.

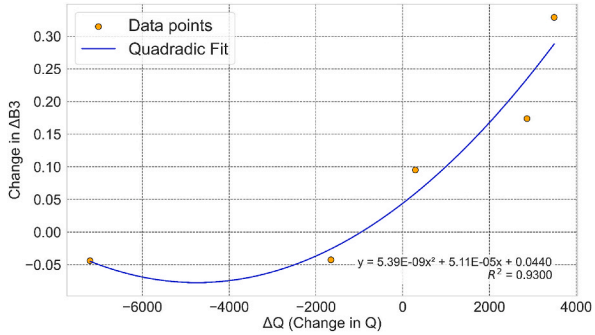


**Fig. 14.** Koshi River reach illustrating changes in channel width configuration relative to flooding discharge, with a quadratic fit applied.

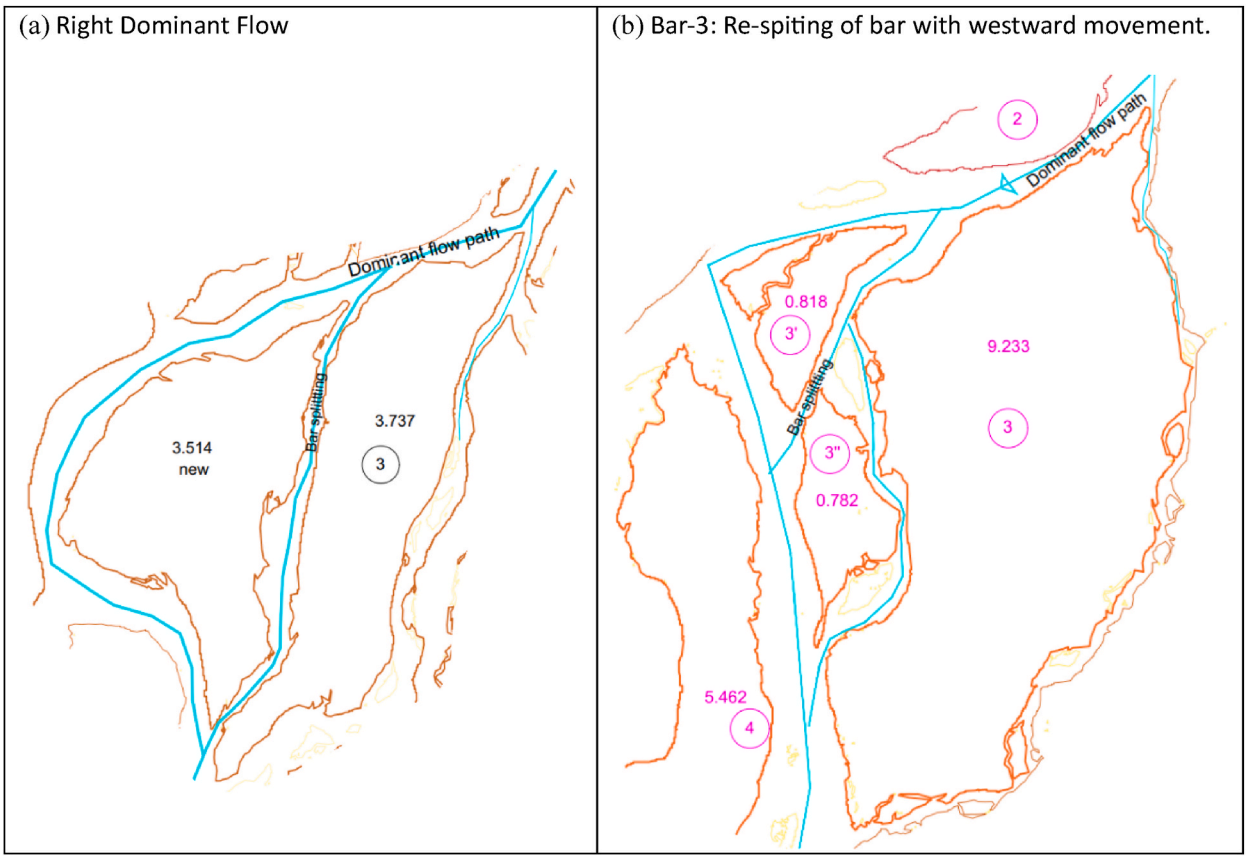


**Fig. 15.** Koshi reach bar number 3 undergoing morphological change with (a) bar splitting on year 2021 with right dominant flow and (b) re-splitting of bar with westward movement at year 2022.

dominant inflow from bar-1, as previously discussed. Also, bar-3 experienced significant growth in size during this period, expanding from 3.737 $km^2$ to 9.233 $km^2$. This growth is primarily attributed to the substantial deposition resulting from the non-dominant flow, specifically the leftward flow in this context.

This movement of bar 1 and 3 implies a progressive westward migration of the main channel. This shift is primarily driven by the growing occurrence of the right flow path, resulting from the higher difference in flooding discharge. This dominance triggers the subdivision of the bar area, subsequently giving rise to the emergence of new flow paths. As time progresses, these nascent pathways undergo continued development, ultimately ending in the breaking of the sand bars in alignment with the prevailing right-oriented flow.

Likewise, in the case of bar-3, a substantial degree of bar movement was observed (Fig. 16). The magnitude of this bar shift resonates with variations in flooding discharge, indicating that higher differences in flooding discharge led to more pronounced channel shift.

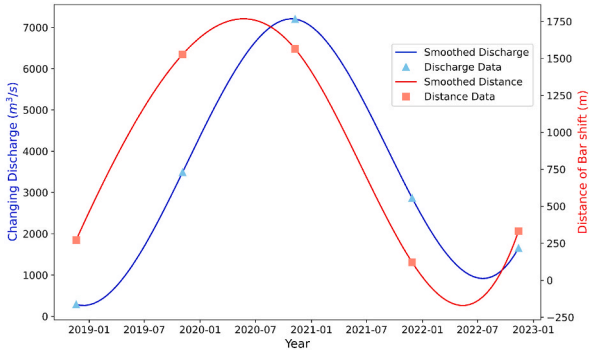


**Fig. 16.** Koshi river's bar number 3 illustrating the magnitude of bar shift over time, reflecting surface changes in response to varying flooding discharge.

## 5. Discussion on comparative study of three rivers

Nepal's rainfall is governed chiefly by the summer monsoon from the Indian Ocean, but its influence is not spatially uniform. A clear east-west gradient is evident: monsoon forcing is weaker in the western Karnali basin than in the eastern Koshi basin (Pokharel et al., 2020). This differential impact is evident in soil erosion rates, where the eastern Koshi basin shows significantly higher rates of erosion 22 t $ha^{-1}$ $year^{-1}$ (Uddin et al., 2016) compared to 9.85 t $ha^{-1}$ $year^{-1}$ in the Karnali basin (Aryal et al., 2023). These data suggest more dynamic river morphology in the downstream regions of the Koshi river compared to the Karnali River. Our study findings comply with these previously done studies where from 1990 to 2022, the Koshi river exhibits the most dynamic morphology, with only 32.5 % of its area remaining unchanged, compared to 64.8 % for the Narayani River and 54.5 % for the Karnali River. The Koshi river also shows significant westward channel shifts, with cumulative planar water area changes of up to 3871 m. These shifts are likely influenced by the high incidence of rainfall-triggered landslides within the Koshi basin, which recorded 5858 landslides, and the 2015 Gorkha earthquake, which triggered 14,127 landslides within the basin alone (Zhang et al., 2019). The significant water area shift between 2000 and 2010 is also linked to the August 2008 flooding when the river breached at Kusaha, Sunsari.

In addition to hydrological drivers, the comparative morphological behavior of the Koshi, Narayani, and Karnali rivers is also strongly governed by sedimentological factors. The Koshi River, with its relatively low slope and extremely high sediment yield (nearly 100 million tons/year) (Sinha et al., 2019), is prone to frequent channel avulsions and lateral instability. Its bed is composed predominantly of quartz-rich sand and gravel (Sharma et al., 2019), and sparse riparian vegetation further reduces bank resistance. In contrast, the Narayani River experiences a more moderated sediment regime, with mixed bed material ranging from coarse sand to gravel and better-developed riparian vegetation, contributing to higher channel stability. The Karnali River, with steep upper slopes and coarse sediment inputs driven by landslides and monsoonal erosion pulses, shows localized braiding in upstream reaches. However, mid-reach vegetation acts to buffer channel migration and dampens lateral shifts.

Over the past two decades, land cover changes have further influenced downstream river morphology in the Koshi, Narayani, and Karnali basins. The Koshi basin saw a 396.10 % increase in built-up areas, indicating urbanization that likely altered runoff and flood dynamics. The reduction in riverbed areas by 13.77 % in Koshi, 87.45 % in Narayani, and 43.01 % in Karnali suggests significant human interventions impacting sedimentation and erosion. These anthropogenic changes, along with shifts in cropland and forest cover, have contributed to the dynamic nature of these river systems.

Also, the Karnali megafan, with its larger valley area, exhibits the highest average erosion rate at 2.322 $km^2$/year, followed by the Koshi river at 1.629 $km^2$/year, and the Narayani River at 1.602 $km^2$/year. This dynamic nature is further illustrated by plotting real-time discharge data against dimensionless $A/L^2$ (Fig. 17) where A is the wetted area and L is the straight reach length. A comprehensive analysis of 180 Sentinel-2 satellites images from 2017, alongside corresponding real-time discharge data, revealed that the Narayani River had the lowest flooding area response to increasing discharge, while the Koshi and Karnali rivers showed significant increases. At a common discharge of 10,000 $m^3$/s, the Koshi River was approximately 39 % more sensitive, and the Karnali River about 33 % more sensitive than the Narayani, underscoring their distinct morphological responses.

While the findings are supported across multiple sensors and decades, several limitations should be noted. Reliance on long-term satellite archives entails uneven temporal sampling and occasional cloud contamination, restricting strict like-for-like comparisons among rivers and years. Because of the large spatial extent, full field-based validation and detailed accuracy checks could not be carried out. The lack of sediment grain size and load data also limited the precision of sediment-related interpretations. By focusing primarily on upstream discharge as the key driver of morphological response, the study could not fully isolate or quantify the influence of other contributing factors, such as structural interventions or subtle natural forces like Coriolis effects. Recognizing these limitations, future research should integrate in-situ validation, sediment characterization, and structural inventories to improve the robustness of RS based assessments of river morphology.

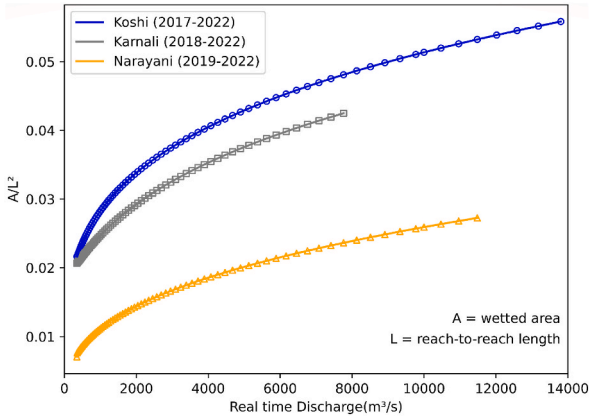


**Fig. 17.** Sensitivity analysis of Koshi, Karnali, and Narayani rivers to changing flood discharge. Each curve follows a power-law relationship between discharge and the wetted area.

## 6. Conclusion

This study offers a comprehensive analysis of morphological changes in Nepal's three major rivers: the Koshi, Narayani, and Karnali over the period 1990 to 2022. By utilizing RS techniques and GIS tools, riverine planform dynamics were systematically mapped and analyzed. The application of satellite-derived indices such as MNDWI and NDWI within the GEE platform enabled the extraction of water bodies, facilitating multi-scale assessments at both decadal and sub-reach levels.

Results reveal distinct variations in channel stability, with the Narayani River displaying the highest proportion of unchanged areas, followed by the Karnali and Koshi Rivers. Braiding intensity analyses in the Koshi and Narayani Rivers indicated a polynomial relationship between $BI_{T3}$ and wetted area, with peak values occurring at intermediate flows and attenuation at higher discharges. These findings suggest a non-linear response of braiding to hydrological variability.

The study also highlights dynamic sandbar behavior along the Koshi River, where westward migration and bifurcation asymmetry were consistently observed from 2017 to 2022. These morphological adjustments were associated with post-monsoonal discharge patterns, right-dominant flow paths, and progressive sandbar splitting.

Overall, the results emphasize the inherent instability and spatial variability of Himalayan braided rivers. The integration of long-term satellite data with discharge records provides a robust framework for interpreting fluvial adjustments in rapidly evolving river systems. These insights contribute to the broader understanding of river planform evolution in complex mountain environments.

## CRediT authorship contribution statement

**Bishwas Bhatta:** Writing – original draft, Software, Methodology, Investigation, Formal analysis, Data curation. **Umesh Singh:** Supervision, Investigation, Formal analysis, Conceptualization. **Basanta Raj Adhikari:** Writing – review & editing, Validation, Resources. **Saroj Karki:** Writing – review & editing, Project administration. **Astha Bhatta:** Writing – review & editing, Visualization.

## Ethical statement

This research, titled " Tracing Morphological Transformations and Braiding Dynamics in the Himalayan Rivers of Nepal" was conducted in adherence to ethical principles and standards for scientific research. The study did not involve any direct human or animal subjects. All satellite imagery and geographic data utilized were obtained from publicly accessible sources, such as Landsat and Sentinel-2 archives, ensuring compliance with licensing agreements and data usage policies.

The authors affirm that the research was carried out with the utmost integrity, transparency, and academic honesty. Any external data or methodologies used have been appropriately cited and acknowledged. This work is original and has not been submitted or published elsewhere in part or full.

There are no conflicts of interest, financial or otherwise, associated with this research. The findings and interpretations presented are solely the authors' and aim to contribute to the scientific understanding of river morphology for sustainable management.

All authors hereby confirm that this research complies with ethical standards, with no conflicts of interest, and is submitted with full transparency and academic integrity.

## Declaration of competing interest

The authors declare that they have no known competing financial interests or personal relationships that could have appeared to influence the work reported in this paper.

## Acknowledgements

The authors express their sincere gratitude to the Department of Hydrology and Meteorology (DHM), Nepal, for providing the streamflow data used in this study. The authors also extend their appreciation to the anonymous reviewers for their valuable feedback and constructive comments.

## Data availability

Data will be made available on request.

## References

Andermann, C., Bonnet, S., Crave, A., Davy, P., Longuevergne, L., Gloaguen, R., 2012. Sediment transfer and the hydrological cycle of himalayan Rivers in Nepal. C. R. Geosci. 344 (11), 627–635. https://doi.org/10.1016/j.crte.2012.10.009.

Aryal, K.R., Panthi, S., Basukala, R.K., Kharel, R., Gautam, A., Poudel, B., Sharma, S., Adhikari, B., Budha, R.K., Khadka, S., Pariyar, S., 2023. Soil loss estimation of karnali river basin, Nepal. Journal of Sedimentary Environments 8 (3), 409–423. https://doi.org/10.1007/s43217-023-00140-y.

Ashmore, P., 2013. Morphology and dynamics of braided RIvers. Treatise on Geomorphology 9 (Chapter 17), 289–312. https://doi.org/10.1016/B978-0-12-374739-6.00242-6.

Azzari, G., Lobell, D.B., 2017. Landsat-based classification in the cloud: an opportunity for a paradigm shift in land cover monitoring. Rem. Sens. Environ. 202, 64–74. https://doi.org/10.1016/j.rse.2017.05.025.

Bajracharya, S.R., Maharjan, S.B., Shrestha, F., Guo, W., Liu, S., Immerzeel, W., Shrestha, B., 2015. The glaciers of the Hindu kush himalayas: current status and observed changes from the 1980s to 2010. Int. J. Water Resour. Dev. 31 (2), 161–173. https://doi.org/10.1080/07900627.2015.1005731.

Baniya, S., Deshar, R., Chauhan, R., Thakuri, S., 2023. Assessment of channel migration of koshi river in Nepal using remote sensing and GIS. Environ. Chall. 11, 100692. https://doi.org/10.1016/j.envc.2023.100692.

Belayneh, Y., Ru, G., Guadie, A., Teffera, Z.L., Tsega, M., 2020. Forest cover change and its driving forces in fagita lekoma district, Ethiopia. J. For. Res. 31 (5), 1567–1582. https://doi.org/10.1007/s11676-018-0838-8.

Bertoldi, W., 2012. Life of a bifurcation in a gravel-bed braided river. Earth Surf. Process. Landf. 37 (12), 1327–1336. https://doi.org/10.1002/esp.3279.

Bertoldi, W., 2021. Braided pattern. In: Hargitai, H., Kereszturi, Á. (Eds.), Encyclopedia of Planetary Landforms. Springer, pp. 1–6. https://doi.org/10.1007/978-1-4614-9213-9_21-1.

Bharati, L., Gurung, P., Maharjan, L., Bhattarai, U., 2016. Past and future variability in the hydrological regime of the koshi basin, Nepal. Hydrol. Sci. J. 61 (1), 79–93. https://doi.org/10.1080/02626667.2014.952639.

Boota, M.W., Yan, C., Idrees, M.B., Li, Z., Soomro, S., Dou, M., Zohaib, M., Yousaf, A., 2021. Assessment of the morphological trends and sediment dynamics in the indus river, Pakistan. J. Water Clim. Change 12 (7), 3082–3098. https://doi.org/10.2166/wcc.2021.125.

Chalov, S.R., Alexeevsky, N.I., 2013. Braided Rivers: structure, types and hydrological effects. Hydrology Reseearch 46 (2), 258–275. https://doi.org/10.2166/nh.2013.023.

Chhetri, R.B., Shakya, N.M., Sitoula, N.R., 2021. Contribution of snow and glacier in hydropower potential and its response to climate change. In: Babel, M., Haarstrick, A., Ribbe, L., Shinde, V.R., Dichtl, N. (Eds.), Water Security in Asia: Opportunities and Challenges in the Context of Climate Change. Springer International Publishing, pp. 207–222. https://doi.org/10.1007/978-3-319-54612-4_16.

Dabojani, D., Mithun, D., Kanti, K.K., 2014. River change detection and bankline erosion recognition using remote sensing and GIS. Forum Geografic XIII (1), 12–17. https://doi.org/10.5775/fg.2067-4635.2014.038.i.

Devreux, L., Chapuis, M., Belletti, B., 2022. Hydromorphological analysis on restored alpine braided Rivers. Geomorphology 415, 108404. https://doi.org/10.1016/j.geomorph.2022.108404.

Dyson, K., Nicolau, A.P., Saah, D., Clinton, N., 2024. Neighborhood-based image transformation. In: Cardille, J.A., Crowley, M.A., Saah, D., Clinton, N.E. (Eds.), Cloud-Based Remote Sensing with Google Earth Engine: Fundamentals and Applications. Springer International Publishing, pp. 195–217. https://doi.org/10.1007/978-3-031-26588-4_10.

Eaton, B.C., Millar, R.G., Davidson, S., 2010. Channel patterns: braided, anabranching, and single-thread. Geomorphology 120 (3), 353–364. https://doi.org/10.1016/j.geomorph.2010.04.010.

Egozi, R., Ashmore, P., 2008. Defining and measuring braiding intensity. Earth Surf. Process. Landf. 33 (14), 2121–2138. https://doi.org/10.1002/esp.1658.

Gorelick, N., Hancher, M., Dixon, M., Ilyushchenko, S., Thau, D., Moore, R., 2017. Google Earth engine: planetary-Scale geospatial analysis for everyone. Rem. Sens. Environ. 202, 18–27. https://doi.org/10.1016/j.rse.2017.06.031.

Grill, G., Lehner, B., Thieme, M., Geenen, B., Tickner, D., Antonelli, F., Babu, S., Borrelli, P., Cheng, L., Crochetiere, H., Ehalt Macedo, H., Filgueiras, R., Goichot, M., Higgins, J., Hogan, Z., Lip, B., McClain, M.E., Meng, J., Mulligan, M., et al., 2019. Mapping the world's free-flowing Rivers. Nature 569 (7755). https://doi.org/10.1038/s41586-019-1111-9. Article 7755.

Hong, L.B., Davies, T.R.H., 1979. A study of stream braiding. GSA Bulletin 90 (12_Part_II), 1839–1859. https://doi.org/10.1130/GSAB-P2-90-1839.

Hooke, J., 2023. Morphodynamics of active meandering Rivers reviewed in a hierarchy of spatial and temporal scales. Geomorphology 439, 108825. https://doi.org/10.1016/j.geomorph.2023.108825.

Hovius, N., Stark, C.P., Allen, P.A., 1997. Sediment flux from a Mountain belt derived by landslide mapping. Geology 25 (3), 231. https://doi.org/10.1130/0091-7613(1997)025<0231:SFFAMB>2.3.CO, 2.

Ibitoye, M.O., 2021. A remote sensing-based evaluation of channel morphological characteristics of part of lower river niger, Nigeria. SN Appl. Sci. 3 (3), 340. https://doi.org/10.1007/s42452-021-04215-1.

Jha, B., Waidbacher, H., Sharma, S., Straif, M., 2010. Study of substrate and physico-chemical base classification of The Rivers of Nepal. Geo Spatial Inf. Sci. 13 (1), 70–76. https://doi.org/10.1007/s11806-010-0126-z.

Kafle, M.R., 2019. Sediment transport measurement in the koshi river: comparison between historic and recent measurement results. American Journal of Water Science and Engineering 5 (3). https://doi.org/10.11648/j.ajwse.20190503.12. Article 3.

Kafle, M.R., 2021. Critical review and improvement of bank protection methods in Nepalese Rivers. J. Inst. Eng. 16 (1). Article 1.

Karki, S., Acharya, S., Gautam, A.R., 2023. Evaluation of vertical accuracy of open access DEMs across different physiographic regions and river basins of Nepal. Earth Science Informatics 16 (4), 3745–3764. https://doi.org/10.1007/s12145-023-01114-4.

Li, Z., Lu, H., Gao, P., You, Y., Hu, X., 2020. Characterizing braided Rivers in two nested watersheds in the source region of the yangtze river on the Qinghai-Tibet Plateau. Geomorphology 351, 106945. https://doi.org/10.1016/j.geomorph.2019.106945.

Li, Z., Yan, C., Boota, M.W., 2022. Review and outlook of river morphology expression. J. Water Clim. Change 13 (4), 1725–1747. https://doi.org/10.2166/wcc.2022.449.

MacClune, K., Yadav, S., Venkateswaran, K., Maharjan, R., Dixit, K.M., Dugar, S., 2014. Urgent Case of Recovery: what We Can Learn from the August 2014 Karnali River Floods in Nepal.

McFEETERS, S.K., 1996. The use of the normalized difference water index (NDWI) in the delineation of open water features. Int. J. Rem. Sens. 17 (7), 1425–1432. https://doi.org/10.1080/01431169608948714.

Mir, Y., Dubeau, F., 2015. Least squares fitting of the stage–discharge relationship using smooth models with curvilinear asymptotes. Hydrol. Sci. J. 60 (10), 1797–1812. https://doi.org/10.1080/02626667.2014.935779.
Mosley, M.P., 1981. Semi-determinate hydraulic geometry of river channels, south island, New Zealand. Earth Surf. Process. Landf. 6 (2), 127–137. https://doi.org/10.1002/esp.3290060206.
Muzzammil, M., Alam, J., Zakwan, M., 2018. A spreadsheet approach for prediction of rating curve parameters. In: Singh, V.P., Yadav, S., Yadava, R.N. (Eds.), Hydrologic Modeling. Springer, pp. 525–533. https://doi.org/10.1007/978-981-10-5801-1_36.
Neupane, P., Karki, S., Bhattarai, P., Pandey, V., Giri, S., 2022. Hydromorphological Characterization of Koshi River on Lower Alluvial Reach.
Nones, M., 2021. Remote sensing and GIS techniques to monitor morphological changes along the middle-lower vistula River, Poland. Int. J. River Basin Manag. 19 (3), 345–357. https://doi.org/10.1080/15715124.2020.1742137.
Pokharel, B., Wang, S.-Y.S., Meyer, J., Marahatta, S., Nepal, B., Chikamoto, Y., Gillies, R., 2020. The east–west division of changing precipitation in Nepal. Int. J. Climatol. 40 (7), 3348–3359. https://doi.org/10.1002/joc.6401.
Pradhan, C., Chembolu, V., Dutta, S., Bharti, R., 2021. Role of effective discharge on morphological changes for a regulated macrochannel river system. Geomorphology 385, 107718. https://doi.org/10.1016/j.geomorph.2021.107718.
Rakhal, B., Adhikari, T.R., Sharma, S., Ghimire, G.R., 2021. Assessment of channel shifting of karnali megafan in Nepal using remote sensing and GIS. Annals of GIS 27 (2), 177–188. https://doi.org/10.1080/19475683.2021.1871950.
Saikia, J., Hazarika, A., Barsha Borah, P., Kumari Shah, R., Protushi Buragohain, P., Saikia, C., Saikia, S., 2024. An interactive study of the brahmaputra river and dibru saikhowa national park of assam using geo-spatial technology and ARIMA model. Catena 241, 108040. https://doi.org/10.1016/j.catena.2024.108040.
Schuurman, F., Ta, W., Post, S., Sokolewicz, M., Busnelli, M., Kleinhans, M., 2018. Response of braiding channel morphodynamics to peak discharge changes in the upper yellow river. Earth Surf. Process. Landf. 43 (8), 1648–1662. https://doi.org/10.1002/esp.4344.
Singh, K.V., Setia, R., Sahoo, S., Prasad, A., Pateriya, B., 2015. Evaluation of NDWI and MNDWI for assessment of waterlogging by integrating digital elevation model and groundwater level. Geocarto Int. 30 (6), 650–661. https://doi.org/10.1080/10106049.2014.965757.
Sinha, R., Gupta, A., Mishra, K., Tripathi, S., Nepal, S., Wahid, S.M., Swarnkar, S., 2019. Basin-scale hydrology and sediment dynamics of the kosi River in the himalayan foreland. J. Hydrol. 570, 156–166. https://doi.org/10.1016/j.jhydrol.2018.12.051.
Smith, S., Lasdon, L., 1992. Solving large sparse nonlinear programs using GRG. ORSA J. Comput. 4 (1), 2–15. https://doi.org/10.1287/ijoc.4.1.2.
Surian, N., 2015. Fluvial processes in braided Rivers. In: Rowiński, P., Radecki-Pawlik, A. (Eds.), Rivers – Physical, Fluvial and Environmental Processes. Springer International Publishing, pp. 403–425. https://doi.org/10.1007/978-3-319-17719-9_15.
Tockner, K., Paetzold, A., Karaus, U., Claret, C., Zettel, J., 2006. Ecology of braided Rivers. In: Braided Rivers. John Wiley & Sons, Ltd, pp. 339–359. https://doi.org/10.1002/9781444304374.ch17.
Tomsett, C., Leyland, J., 2019. Remote sensing of river corridors: a review of current trends and future directions. River Res. Appl. 35 (7), 779–803. https://doi.org/10.1002/rra.3479.
Uddin, K., Murthy, M.S.R., Wahid, S.M., Matin, M.A., 2016. Estimation of soil erosion dynamics in the koshi basin using GIS and remote sensing to assess priority areas for conservation. PLoS One 11 (3), e0150494. https://doi.org/10.1371/journal.pone.0150494.
van Vliet, M.T.H., Franssen, W.H.P., Yearsley, J.R., Ludwig, F., Haddeland, I., Lettenmaier, D.P., Kabat, P., 2013. Global river discharge and water temperature under climate change. Glob. Environ. Change 23 (2), 450–464. https://doi.org/10.1016/j.gloenvcha.2012.11.002.
Xu, H., 2006. Modification of normalised difference water index (NDWI) to enhance open water features in remotely sensed imagery. Int. J. Rem. Sens. 27 (14), 3025–3033. https://doi.org/10.1080/01431160600589179.
Xu, X., Xu, S., Jin, L., Song, E., 2011. Characteristic analysis of otsu threshold and its applications. Pattern Recognit. Lett. 32 (7), 956–961. https://doi.org/10.1016/j.patrec.2011.01.021.
Yang, X., Chen, Y., Wang, J., 2020. Combined use of Sentinel-2 and landsat 8 to monitor water surface area dynamics using google Earth engine. Remote Sensing Letters 11 (7), 687–696. https://doi.org/10.1080/2150704X.2020.1757780.
Yaraghi, N., Ronkanen, A., Darabi, H., Kløve, B., Torabi Haghighi, A., 2019. Impact of managed aquifer recharge structure on river flow regimes in arid and semi-arid climates. Sci. Total Environ. 675, 429–438. https://doi.org/10.1016/j.scitotenv.2019.04.253.
Yigez, B., Xiong, D., Zhang, B., Yuan, Y., Baig, M.A., Dahal, N.M., Guadie, A., Zhao, W., Wu, Y., 2021. Spatial distribution of soil erosion and sediment yield in the koshi river basin, Nepal: a case study of triyuga watershed. J. Soils Sediments 21 (12), 3888–3905. https://doi.org/10.1007/s11368-021-03023-9.
Zhang, J., van Westen, C.J., Tanyas, H., Mavrouli, O., Ge, Y., Bajrachary, S., Gurung, D.R., Dhital, M.R., Khanal, N.R., 2019. How size and trigger matter: analyzing rainfall- and earthquake-triggered landslide inventories and their causal relation in the koshi river basin, central himalaya. Nat. Hazards Earth Syst. Sci. 19 (8), 1789–1805. https://doi.org/10.5194/nhess-19-1789-2019.